Biochimica et Biophysica Acta, 936 (1988) 269–279
Elsevier

BBA 42873

Chemical modification of the active site of ferredoxin–NADP$^+$ reductase and conformation of the binary ferredoxin/ferredoxin–NADP$^+$ reductase complex in solution

Enno C. Apley and Richard Wagner

Biophysik, Fachbereich Biologie/Chemie, Universität Osnabrück, Osnabrück (F.R.G.)

(Received 17 March 1988)
(Revised manuscript received 13 June 1988)

Key words: Photosynthesis; Electron transport; Ferredoxin–NADP$^+$ reductase; NADP binding site; Ferredoxin; Rotational diffusion

Ferredoxin–NADP$^+$ reductase (EC 1.18.1.2) was chemically modified by the triplet probe eosin isothiocyanate (eosin-NES). Incorporation of 1 mol eosin-NCS/mol ferredoxin–NADP$^+$ reductase completely inhibited binding of NADP$^+$/NADPH to the enzyme. Binding of eosin without the reactive group to the enzyme was shown to be reversible but to compete with NADP$^+$/NADPH with a K_i of approx. 5 μM. The binding site of eosin-NCS has been located in the primary sequence ferredoxin–NADP$^+$ reductase. After specific cleavage of arginine with trypsin a single labelled peptide was obtained and identified as the fragment from residue 179–228 in the primary sequence. Binding of eosin-NCS occurred in either of two predicted helices (residues 179–189 or 212–228) which are both part of an α/β structure characteristic for nucleotide binding folds. The rotational diffusion in solution of the eosin-labelled ferredoxin–NADP$^+$ reductase and its complex with ferredoxin was measured with laser flash spectroscopy under photoselection. From the measured rotational correlation times and the known structure of ferredoxin–NADP$^+$ reductase at 3.7 Å resolution, we propose that ferredoxin is bound to ferredoxin–NADP$^+$ reductase between the two domains of the flavoprotein. The two ferredoxin–NADP$^+$ reductase domains and ferredoxin form a triangle which results in a highly integrated binary complex.

Introduction

The terminal step of the electron transport chain in chloroplasts, the photoreduction of NADP$^+$, is catalyzed by ferredoxin–NADP$^+$ reductase (EC 1.18.1.2) [1,2]. This flavoprotein is attached to the stromal side of the thylakoid membrane [3], mostly found (86%) in the unstacked membrane regions as determined by immunochemical studies [4]. Ferredoxin–NADP$^+$ reductase seems to be anchored on the membrane via an intrinsic 17.5 kDa membrane protein [5,6]. Ferredoxin–NADP$^+$ reductase receives electrons from PS I via ferredoxin, a water-soluble iron-sulfur protein with molecular mass 11.5 kDa. Ferredoxin–NADP$^+$ reductase mediates electron transfer between the one-electron-carrier ferredoxin and the two-electron-acceptor NADP$^+$. In

Abbreviations: eosin-NCS, eosin 5-isothiocyanate; SDS-PAGE, sodium dodecyl sulphate polyacrylamide gel electrophoresis; DCIP, 2,6-dichlorophenolindophenol; DTT, dithiothreitol; PS I, photosystem I; HPLC, high pressure liquid chromatography; Tricine, *N*-[2-hydroxy-1,1-bis(hydroxymethyl)ethyl]glycine.

Correspondence: R. Wagner, Fachbereich Biologie/Chemie, Universität Osnabrück, Postfach 4469, D-4500 Osnabrück, F.R.G.

aqueous buffers ferredoxin and ferredoxin–$NADP^+$ reductase form 1 : 1 complexes in the different redox states of the two components [7,8]. The reduction kinetics of the ferredoxin/ferredoxin–$NADP^+$ reductase complex has been resolved [9].

Little is known of the quaternary structure of the binary complex between the two proteins. The amino acid sequence of ferredoxin–$NADP^+$ reductase has been determined [13] and the structure of the enzyme has been resolved to 3.7 Å [12]. Ferredoxin–$NADP^+$ reductase has been shown to be a kidney-shaped protein ($30 \times 50 \times 50$ Å) divided into two structural domains, one containing the NADP binding site and the other one the FAD site [12,13]. The nucleotide binding fold in the $NADP^+$ binding domain has been tentatively located in the primary sequence [12,13].

The main purpose of our study was to investigate the structure of the binary ferredoxin/ferredoxin–$NADP^+$ reductase complex. For this the ferredoxin–$NADP^+$ reductase was labelled with the triplet probe eosin-NCS and the rotational diffusion of the labelled ferredoxin–$NADP^+$ reductase and its complex with ferredoxin was measured in different redox states. Based on measured rotational correlation times and on the known structure of ferredoxin–$NADP^+$ reductase the most probable structure of the binary complex is proposed.

The binding of the label to ferredoxin–$NADP^+$ reductase was competitive with NADP and a single peptide was found to be modified. The label was bound in the vicinity of the NADP binding site on either one of two predicted α-helices (residues 179–193 or 212–222), where a predicted α/β-structure forms a topology which is typically observed in nucleotide binding folds [12,13,36].

Materials and Methods

Ferredoxin (from spinach) and horse heart cytochrome *c* were purchased from Sigma and used without Further purification. All other chemicals were of analytical grade.

Preparation of ferredoxin–$NADP^+$ reductase. Ferredoxin–$NADP^+$ reductase was prepared from spinach chloroplasts as described in Ref. 18. By this procedure a homogeneous protein, which gave a single band at 36 kDa on silver stained SDS-PAGE, with a specific diaphorase activity of 20–25 μmol reduced DCIP/mg per min at pH 7.5, 25 °C was obtained.

Labelling of ferredoxin–$NADP^+$ reductase with eosin-NCS. The purified enzyme was labelled with eosin-NCS in a buffer containing 50 mM Tris-HCl (pH 8.0), 50 mM KCl as described [14]. Eosin-NCS (Molecular Probes) was dissolved (1 mg/ml) in 50 mM Tricine buffer (pH 8) and used within 20 min in order to restrict hydrolysis of the -NCS group. The reaction was terminated by the addition of glycine in 100-fold molar excess and the unbound eosin was removed by gel filtration on Sephadex G-25. The amount of protein-bound eosin-NCS was determined by measuring the eosin absorbance at 528 nm, since binding of the dye to the protein did not change the absorption coefficient of $\epsilon = 8.35 \cdot 10^4\ M^{-1} \cdot cm^{-1}$ [17].

Other methods. Diaphorase activity and cytochrome *c* reduction were measured as described in Ref. 23. Ferredoxin-mediated cytochrome *c* reduction was also determined in the presence of 10–60% v/v glycerol. Viscosity of the buffer was either taken from Ref. 25 or measured in a micro-Uppelohde viscosimeter. Protein was determined by the Coomassie-binding method as described in Ref. 21. Difference spectra were recorded in a Hitachi 150-20 spectrophotometer by the use of two tandem cells, which contained separated volumes of enzyme and ligand in the reference cell and equal but mixed volumes in the sample cell.

Arginine specific cleavage of eosin-labelled ferredoxin–$NADP^+$ reductase. Gel filtration of 200 nmol of DTT-reduced ferredoxin–$NADP^+$ reductase was carried out against 6 M guanidine-HCl and 40 mM Na_2HPO_4 (pH 8.8), final volume 3.5 ml. 100 μl citraconic anhydride (Eastman Kodak) were added, while the pH was kept constant by addition of NaOH. After 30 min incubation, buffer was changed by gel filtration to 100 mM NH_4HCO_3 (pH 8.8) and the enzyme digested by incubation with 100 μg TPCK-trypsin (Sigma) for 2 h at 37 °C. Peptides were decitraconylated in 30% HCOOH for 3 h at 37 °C and lyophilized.

Reversed phase HPLC chromatography of the arginine fragments was performed on a reversed phase column (C_1/C_8, Pro RPC HR 5/10, Pharmacia). The column was equilibated with 0.1%

(w/v) trifluoroacetic acid (buffer A) and the sample was eluted with a linear gradient of acetonitrile (buffer B; 0–50% in 60 min) at a flow rate of 0.6 ml/min. Absorption of the peptides in the eluate was monitored at 214 nm and 518 nm.

Elution peaks of the eluate were analyzed for their amino acid composition by standard procedures [38]. The relative amount of each amino acid residue was compared to the expected amounts of the same residue in the 10 arginine fragments as calculated from the known amino acid sequence [13]. The square sum for the difference of estimated and the theoretical expected amino acid composition was computed to detect similarity between the given 10 amino acid compositions and the estimated amino acid compositions of the eosin-containing peak. The following equation was used:

$$\text{relative deviation} = \sum_{\text{Ala}}^{\text{Val}} (\kappa - \lambda)^2$$

where κ is the relative abundance of a particular amino acid and λ the experimental observed value for the same amino acid. The relative retention times of the 10 expected ferredoxin–$NADP^+$ reductase digestion fragments under the above column flow conditions were calculated as described in detail in Ref. 35.

Laser flash spectroscopy. The principles and geometrical features for measuring rotational diffusion of macromolecules with extrinsic probes by the photoselection technique are given in detail elsewhere [17,20]. The eosin absorption changes at 502 nm due to ground state depletion and its subsequent repopulation from the triplet state were used for measurement [17]. The sample was excited (up to 30% saturation) with flashes from a frequency-doubled Q-switched Nd-Yag laser (5 ns pulse duration, fwhm). The d.c. output of the detection photodiode was digitized (Biomation 6500) and the transients averaged on a Tracor TN 1500 computer. The absorption changes $\Delta A_{\parallel}(t)$ and $\Delta A_{\perp}(t)$ for parallel and perpendicular polarisation of the E-vector of exciting and measuring light yielded the time course of the absorption anisotropy according to:

$$r(t) = \frac{\Delta A_{\parallel}(t) - \Delta A_{\perp}(t)}{\Delta A_{\parallel}(t) + 2\Delta A_{\perp}(t)} \qquad (1)$$

The total absorption change reflects the ground state depletion and its subsequent repopulation from the triplet state (triplet lifetime) without interference of rotational diffusion. The absorption anisotropy reflects the rotational diffusion only [17,24]. The data were processed on a PDP 11/34 computer and analysed for their amplitudes and decay times as described in detail elsewhere [15,17,20]. The sample in a 1 ml, 1 cm optical lightpass cuvette contained 10–24 nmol of ferredoxin–$NADP^+$ reductase (1 mol eosin bound/mol enzyme) and a 2–5-fold excess of ferredoxin in a buffer containing 50 mM Tris-HCl (pH 8.0), 20 mM KCl and 25% (v/v) glycerol. All measurements were performed at 20 °C.

Calculation of the theoretical rotational correlation times for oligomeric model structures were performed as described in detail elsewhere [20]. The rotational diffusion coefficient for the model structures were taken from Ref. 19.

Results and Discussion

Modification of the enzyme with eosin-NCS

The isolated and purified enzyme was modified with the triplet label eosin-NCS. Fig. 1 shows the binding of eosin-NCS as function of the incubation time at a given eosin-NCS concentration (100 μM). The graph comprises two different components: at the beginning rapid binding of eosin-NCS to the enzyme occurs up to an eosin load of 1 mol dye/mol protein; further binding (up to > 2 mol dye/mol protein) occurred at a much slower rate.

The labelled ferredoxin–$NADP^+$ reductase did not produce the characteristic difference spectrum with NADP [31], which indicated that NADP did not bind to the enzyme after modification. In agreement with this observation binding of 1 mol eosin/mol ferredoxin–$NADP^+$ reductase resulted in a complete loss of diaphorase activity as shown in Fig. 2.

In contrast to the results described earlier for the labelling with eosin-NCS [14], upon prolonged incubation (≥ 5 min) it was not possible to achieve complete protection of the enzyme against inactivation by the label with $NADP^+$ or NADPH even at high concentrations (100 mM). This discrepancy was presumably due to different enzyme preparation protocols used in the former experi-

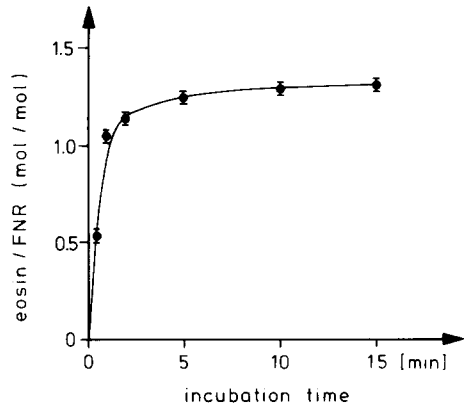

Fig. 1. Binding of eosin-NCS to ferredoxin–NADP$^+$ reductase (FNR) as function of time. 0.7 mg/ml ferredoxin–NADP$^+$ reductase was incubated in a reaction medium containing 50 mM Tricine (pH 8.0) and 100 μM eosin-NCS. At the indicated times 1 ml aliquots were withdrawn and the reaction stopped by the addition of 100 μl 1 M glycine. The aliquots were passed through a Sephadex G-25 column (Pharmacia PD 10) in order to remove unbound eosin-NCS. Protein and protein-bound eosin-NCS were determined as described in the Materials and Methods section.

ments. In our previous work we have shown that a chloroform preparation procedure may yield a ferredoxin–NADP$^+$ reductase apparently lacking a 3 kDa peptide [18]. Preliminary sequence data (B. Wittmann-Liebold and S. Engelbrecht, unpublished) revealed that the protein we used in these actual experiments was identical to the integral ferredoxin–NADP$^+$ reductase described by Karplus et al. [13] and that the preparations producing a 33 kDa and a 36 kDa band on SDS-PAGE seemed to be composed of the complete enzyme containing 314 amino acid residues, whereas the 33 kDa band seemed to contain the enzyme lacking peptides of different lengths at the N-terminus (see also Ref. 13).

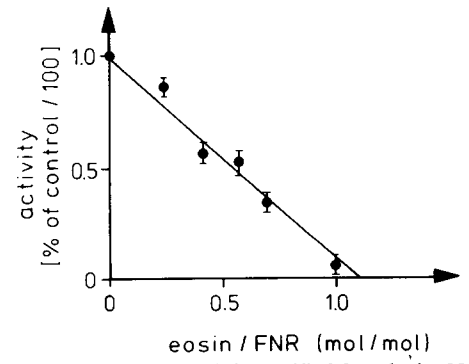

Fig. 2. Diaphorase activity of the purified ferredoxin–NADP$^+$ reductase (FNR) as a function of the amount of bound eosin-NCS. Control activity of the unlabelled protein (100%) corresponded to a specific activity of 21.9 μmol reduced DCIP/mg per min. Covalent labelling of the enzyme with eosin-NCS was performed essentially as described in the legend to Fig. 1.

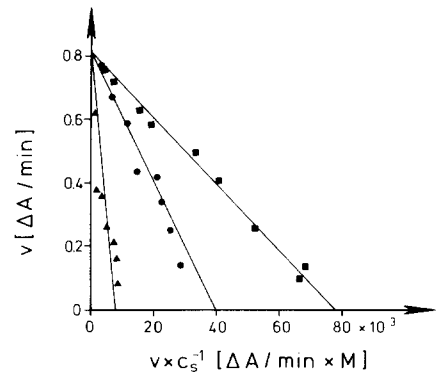

Fig. 3. Woolf-Augustinsson-Hofstee plot of the rate of ferredoxin–NADP$^+$ reductase diaphorase activity with variable concentrations of NADP$^+$ (2–500 μM) in the absence (■) and presence of 5 μM hydrolyzed eosin (●) and 20 μM eosin (▲). The DCIP reduction (ΔA/min) was measured at 595 nm.

Eosin (without the reactive -NCS group) still was strongly bound in a non-covalent way to ferredoxin–NADP$^+$ reductase. This could be inferred from the difference spectra of eosin and the enzyme, which showed a shift of the eosin absorption maximum from 525 nm to 535 nm, indicating strong electrostatic interaction between the dye and the protein (not shown). To investigate the effect of non-covalent eosin binding on the enzyme activity, binding of eosin to the enzyme was measured via ferredoxin–NADP$^+$ reductase-mediated DCIP reduction with variable concentrations of NADP$^+$ and in the presence and absence of eosin. The results of these measurements are shown in Fig. 3, where the velocities v of the diaphorase reaction (ΔA/min) are plotted versus v/c_s according to Woolf-Augustinsson-Hofstee [32]. In the absence of eosin the K_m for NADPH was approx. 10 μM. This value is in good agreement with values previously reported in the literature [2]. In the presence of eosin the apparent K_m increases whereas v_{max} is not affected. Obviously eosin inhibits NADP binding competitively. This competitive inhibition shows that eosin binds at or

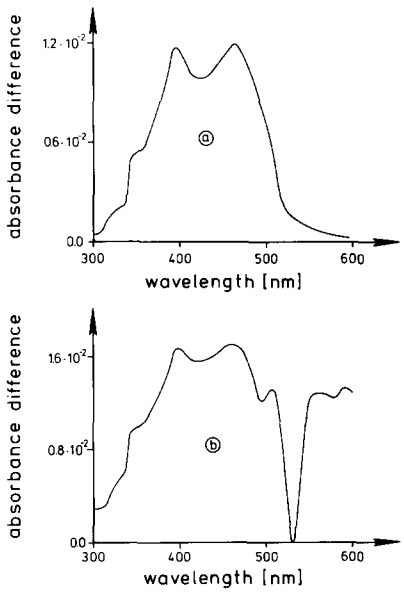

Fig. 4. (a) Difference mixing spectrum of isolated and purified ferredoxin–$NADP^+$ reductase (13.7 μM) with ferredoxin (17.4 μM) in a buffer containing 50 mM Tricine (pH 8), 20 mM KCl. (b) shows a spectrum as in (a) but eosin-NCS-labelled ferredoxin–$NADP^+$ reductase at a concentration of 11 μM was used. Both spectra were recorded with two tandem cells. The sample cuvette contained both complex-forming proteins in the first compartment and an equal volume of buffer in the second. The reference cuvette contained equal volumes of ferredoxin–$NADP^+$ reductase and ferredoxin separated in the two compartments.

close to the enzyme's nucleotide binding fold. The low K_i of approx. 5 μM, as estimated from the data shown in Fig. 3, compared to the K_m of 10 μM indicates that eosin is rather strongly bound at the active site. This result also explains why NADP was not able to protect the enzyme completely from inactivation by eosin-NCS, Although with the above $K_i \approx 5$ μM for eosin, NADP in principle should protect the enzyme against inactivation by eosin-NCS. However the protection will disappear at longer incubation times since covalent binding of eosin-NCS irreversibly removes enzyme from the competitive binding equilibrium. Together these results indicate that eosin-NCS is covalently bound at the nucleotide binding site by reacting with a lysine residue at or near this site.

Fig. 4a shows the difference spectrum of the native ferredoxin–$NADP^+$ reductase upon binding of ferredoxin in a binary complex [10]. In Fig. 4b eosin-NCS-modified ferredoxin–$NADP^+$ reductase (1 mol eosin-NCS/mol protein) was used instead of the native enzyme. In the wavelength region from 300 nm to 500 nm, where the chromophores of the two proteins absorb, the spectrum is identical to that in Fig. 4a. However above 500 nm additional peaks due to absorption differences induced by ferredoxin binding in the eosin band appear. It is evident from the spectra in Fig. 4 that binding of ferredoxin to the ferredoxin–$NADP^+$ reductase is not abolished by the covalently bound label. In spite of that, covalently bound eosin-NCS 'recognizes' binding of ferredoxin to ferredoxin–$NADP^+$ reductase by showing a shift of its absorbance peak in difference spectra.

Peptide mapping

Eosin-NCS-labelled ferredoxin–$NADP^+$ reductase was subjected to peptide mapping in order to locate the eosin binding site in the primary sequence. From the known primary sequence of ferredoxin–$NADP^+$ reductase [13] only 10 peptides are to be expected upon arginine-specific trypsin cleavage. We performed the cleavage after blocking lysine residues by citraconylation. The obtained arginine fragments were separated on a C_1/C_8 reversed phase column with a linear gradient of acetonitrile (buffer B). The absorption of the eluate was monitored at 214 and 518 nm respectively. Fig. 5 shows a typical chromatogram. In the elution profile obtained for the trypsin-digested ferredoxin–$NADP^+$ reductase at 214 nm eight major peaks (with a broad peak at approx. 45% buffer B) appeared with increasing concentration of acetonitrile in the elution buffer (see Fig. 5A, a) whereas at 518 nm only one major rather broad peak at approx. 45% buffer B appeared. We calculated the relative retention times for the 10 ferredoxin–$NADP^+$ reductase peptides in the reversed phase column as described in Ref. 35; the result of this calculation is shown at the bottom of Fig. 5. From the results of these calculations the broad peak monitored at approx. 45% acetonitrile may be tentatively assigned to the unresolved largest peptide fragments F5, F6 or F9 (see Fig. 5). The broad peak as monitored at 518 nm of several runs was pooled and rechromatographed with a linear gradient from 30–60% buffer B. This is shown in Fig. 5B. Again at 214 nm a (rather

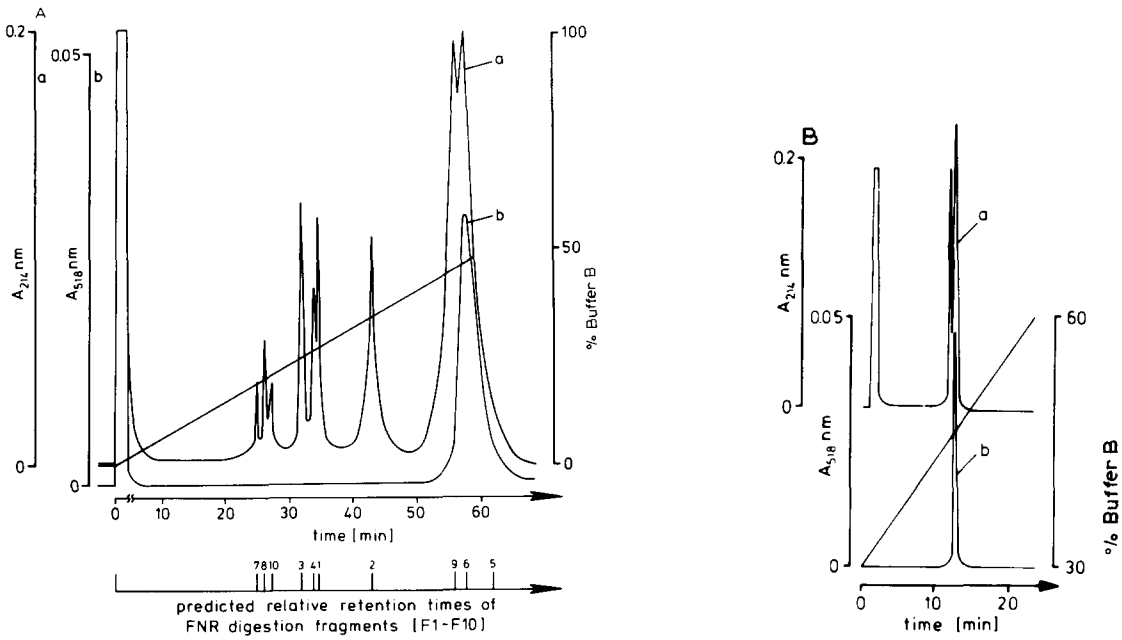

Fig. 5. (A) Chromatogram of HPLC reversed phase run of ferredoxin–$NADP^+$ reductase (FNR) digestion fragments. 200 μg of lyophilized peptides were dissolved in 500 μl of a 1:1 mixture of 50% CH_3COOH and CH_3OH. 100 μl of this solution were applied to the column (ProRPC HR 5/10, Pharmacia) which had been equilibrated with buffer A (0.1% (w/v) trifluoroacetic acid). The sample was eluted with a linear gradient of 0–50% acetonitrile at a flow rat of 0.6 ml/min. In chromatograms (a) and (b) identical samples were applied, however in (a) elution was monitored at 214 nm, whereas in (b) elution was monitored at 518 nm. (B) Shows the elution profile obtained for the second run of peak b in the reversed phase column. Again identical samples monitored at 214 (a) and 518 nm (b) are shown. Below the chromatogram relative retention times on reversed phase column calculated for ferredoxin–$NADP^+$ reductase digestion fragments F1–F10 is shown (for details see text).

broad) peak with two distinct shoulders appeared; however at 518 nm a rather narrow peak corresponding to the second shoulder of the 214 nm peak appeared (Fig. 5B, b). The narrow peak at 518 nm was subjected to amino acid composition analysis. The results of the amino acid composition analysis of the eosin-containing peptide are shown in Table I; they were compared with the known composition of all possible ferredoxin–$NADP^+$ reductase fragments by a least-square analysis (see Materials and Methods). The calculation showed that F6 could be identified as the fragment with the highest confidence. Allowing a 20% contamination of F6 with F9 resulted in almost identical amino acid compositions of the theoretical and the analysed HPLC peak (see Table I). Together the above results show that eosin-NCS was covalently bound to the F6 peptide fragment of the ferredoxin–$NADP^+$ reductase. This peptide contains the amino acids at position 179–228 in the primary sequence of ferredoxin–$NADP^+$ reductase.

From X-ray crystallography and secondary structure prediction location of the nucleotide binding site of ferredoxin–$NADP^+$ reductase in the primary sequence has been proposed [12,13]. We also calculated the secondary structure prediction by the method of Garnier et al. [34]. A strand of β-sheet (residues 164–169) and a glycine-rich loop (residues 170–173) are followed by two alternating α-helix (residues 179–189 and 212–228) and β-sheet (residues 195–203 and 228–233) structures.

Although the results of the secondary structure predictions have to be taken with caution [37], they appear to agree with the results of Karplus et al. [13], that the eosin-NCS is bound at an α/β structure characteristic of the nucleotide binding fold. According to the predicted structure and most interestingly, the possible seven lysines in

TABLE I

COMPARISON OF THE CALCULATED AMINO ACID COMPOSITION OF THE F6 PEPTIDE AND THE EXPERIMENTAL EVALUATED AMINO ACID COMPOSITION OF THE EOSIN-CONTAINING HPLC PEAK

The minimum amino acid composition was calculated taking the arginine content (= 1) as reference.

Amino acids	Amino acid composition	
	F6 peptide	eosin-containing peptide
Asx	5	4.4
Thr	1	1.4
Ser	4	3.6
Glx	5	5.2
Pro	2	1.6
Gly	2	1.6
Ala	2	1.6
Val	1	0.8
Met	2	2.2
Ile	0	0.0
Leu	6	5.6
Tyr	2	1.6
Phe	7	5.6
His	1	0.8
Lys	7	6.6
Arg	1	1.0

F6, where eosin-NCS could be bound, are located in the two helices (residues 179–189 and 212–228) which are supposed to be an essential part of the nucleotide binding fold of ferredoxin–$NADP^+$ reductase. Zanetti also reported on the presence of a single essential lysine residue which could be modified by dansyl chloride [39]. The peptide containing the essential lysine modified by dansyl chloride has been identified [40]. Comparison of the peptide sequence [40] with the known sequence of ferredoxin–$NADP^+$ reductase reveals that the peptide can be identified as the amino acid residues 110–117 in the primary sequence of the whole enzyme [13]. The modified lysine then could be assigned to be lysine 116. In contrast to this, Chan et al. [41] identified lysine 244 as another essential amino acid after modification of the protein with periodate-oxidized $NADP^+$. Thus the enzyme seemed to contain at least three different 'essential' lysine residues at position 116 [40], position 244 [41] and one of the seven lysines in residues 178–228 (this paper). These results show that even location of an essential amino acid residue in the primary sequence solely does not provide information on the topology of the active site. To really understand how these groups work as 'essential' ones, the three-dimensional structure of the enzyme at higher resolution is required.

Rotational diffusion

Rotational diffusion of ferredoxin–$NADP^+$ reductase and of its complex with ferredoxin at different redox states was measured. Ferredoxin–$NADP^+$ reductase-bound eosin was used as a spectroscopic probe. Since the time resolution of our laser spectrophotometer was limited to times greater than 20 ns due to the unavoidable flash burst it was necessary to slow down the fast rotation of the proteins by addition of glycerol to the medium. To find conditions where glycerol probably exhibits no secondary effects on the proteins, cytochrome *c* reduction of the ferredoxin/ferredoxin–$NADP^+$ reductase complex was measured as a function of the glycerol concentration. The results are shown in Fig. 6. The decrease in activity was reciprocal to the viscosity and therefore possibly diffusion-limited up to a concentration of approx. 25% (v/v) glycerol (approx. 2 cP). At higher concentrations secondary effects on protein conformation seem to occur. We therefore performed all hydrodynamic measurements in the presence of not greater than 25% (v/v) glycerol in the buffer.

As an example of the original data, Fig. 7 shows transient absorption changes of eosin which were obtained with eosin-NCS-labelled ferredoxin–$NADP^+$ reductase. The upper trace shows the

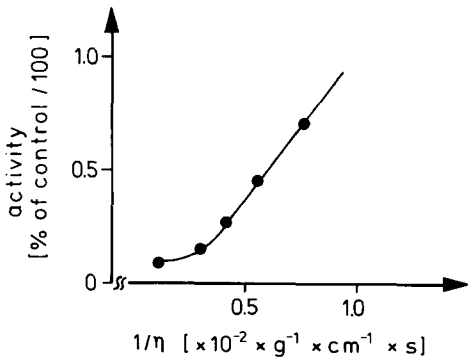

Fig. 6. Ferredoxin–$NADP^+$ reductase-mediated cytochrome *c* reduction in the presence of 0–60% (v/v) glycerol. The relative extent of the cytochrome *c* reduction is plotted as a function of the inverse medium viscosity. Control activity in aqueous buffer at 1 cP was 23 μmol reduced cytochrome *c*/mg per min.

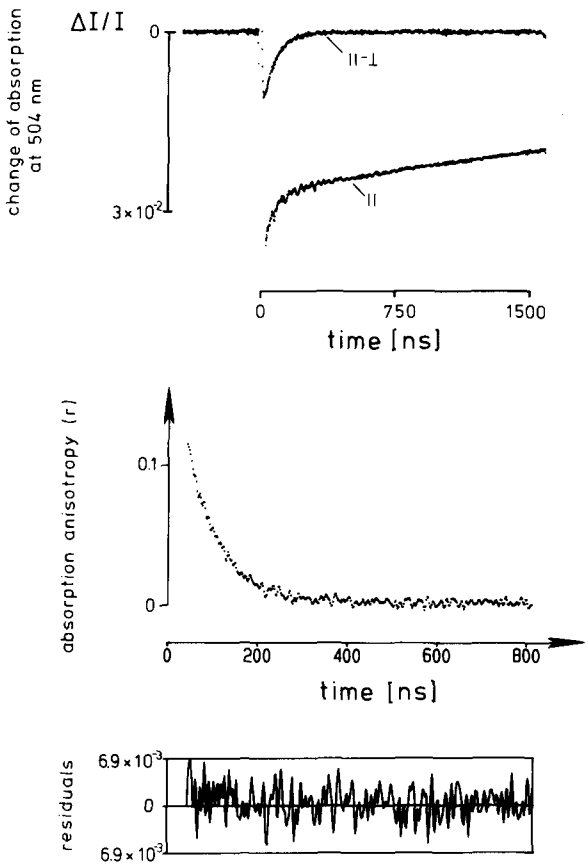

Fig. 7. Top. Time course of the absorption changes of eosin-NCS covalently bound to ferredoxin–NADP$^+$ reductase under parallel polarisation between the measuring light and the excitation flash (trace marked ||) and difference calculated from absorption changes obtained under parallel and perpendicular measuring light (trace marked $\| - \perp$). Protein concentration was 0.54 mg/ml in a buffer containing 50 mM Tricine (pH 8), 20 mM KCl and 25% (v/v) glycerol. Middle. Time course of absorption anisotropy calculated according Eqn. 1 from the above traces. Bottom. Corresponding residuals of the computer fit (see Table II) for the decay of the absorption anisotropy.

time course of the difference of the absorption changes ($\Delta A_{\|}(t) - \Delta A_{\perp}(t)$) at parallel ($\Delta A_{\|}(t)$) and perpendicular ($\Delta A_{\perp}(t)$) polarization of the exciting light relative to the polarization of the interrogating laser beam. The other trace shows the time course of the absorption changes at parallel polarization alone. The middle trace shows the time course of the absorption anisotropy as calculated point by point from the upper two traces (see Eqn. 1, Materials and Methods). The lowest trace in Fig. 7 represents the residuals of a computer fit of the data shown in the middle trace. The results of this and other measurements under various conditions are listed in Table II. The rotational correlation times were measured at a viscosity of 2.095 cP and normalized to the viscosity of water at 20°C (1 cP). The absorption anisotropy of isolated ferredoxin–NADP$^+$ reductase (oxidized form) decayed with a rotational correlation time of 27.7 ns (±0.42 ns). Addition of the reducing agents DTT or sodium dithionite under anaerobic conditions increased the rotational correlation time to 32.7 ns (±0.31 ns). In the presence of ferredoxin the correlation time was 34.3 ns (±0.19 ns) and reduction of the flavoprotein/ferredoxin complex resulted in a further increase to 37.4 ns (±0.43 ns). No effect of NADP$^+$ or NADPH on the rotational correlation times were observed.

To relate the experimentally observed rotational correlation times of macromolecules with possible structures they are compared with the theoretical decay times of model structures. For a sphere the rotation time may be calculated according to:

$$\tau_{sph} = V_{hydr} \cdot \eta / kT \qquad (2)$$

where the hydrated volume is:

$$V_{hyd} = M_r \cdot (v_p + v_s \cdot h) / N_A \qquad (3)$$

and k is the Boltzmann constant, η the viscosity

TABLE II

AMPLITUDES $r(0)$ AND CORRESPONDING ROTATIONAL CORRELATION TIMES τ_{exp} OF FERREDOXIN–NADP$^+$ REDUCTASE AND ITS COMPLEX WITH FERREDOXIN IN THE OXIDIZED AND REDUCED STATE

The values are corrected to the viscosity of water (1 cP). The last row shows the standard deviations of the computerfitted data in NS.

Sample		$r(0)$	τ_{exp} (ns)	S.D.
FNR [a]	(ox.)	0.22	27.7	±0.42
FNR	(red.)	0.21	32.7	±0.31
FNR/Fd [b]	(ox.)	0.22	34.3	±0.19
FNR/Fd	(red.)	0.21	37.4	±0.43

[a] Ferredoxin–NADP$^+$ reductase.
[b] Ferredoxin.

of the medium, v_p and v_s are the partial specific volumes of the protein and the solvent and N_A is Avogadro's number. (With a molecular weight of 35 317 taken from Ref. 13, $v_p = 0.745$ and $h = 0.5$ g water/g protein for a soluble protein, we obtain a hydrated volume of $7.3 \cdot 10^{-20}$ cm^3 and a τ_{sph} of 18.1 ns).

The difference between the theoretical decay time τ_{sph} and the experimental observed time contains information about the deviation of the protein from ideal spherical shape. The deviations are commonly interpreted by relating the diffusion coefficients of the spheres to hydrodynamic model structures with non-spherical shape, oblate or prolate ellipsoids of revolution [30] and arbitrary arrangements of spherical elements [19]. These model structures with at least one symmetry axis reveal two different diffusion coefficients which lead in the case of rotational diffusion to three rotational correlation times. These are weighted by their amplitudes as a function of the angle θ between the absorption transition dipole moment and the main symmetry axis of the protein [30]. Since we observed only one rotational correlation time, we have to conclude that one of the possible three amplitudes was dominating and that the amplitudes of the other two decay components were too small to be resolved. From the dependence of the three amplitudes on the angle θ it is obvious that there exists only one range of θ where one relaxation time is dominating [30]. That is, only τ_1 appears to be dominant around an angle of $\theta \approx 0°$. We therefore tentatively assign our observed correlation time to τ_1.

As the interpretation of rotational correlation times by hydrodynamic model structures is always ambiguous, we used additional information from crystallographic studies, which revealed that ferredoxin–NADP$^+$ reductase has two structural domains of similar size [12]. In those x-ray diffraction studies the kidney-shaped ferredoxin–NADP$^+$ reductase had the rough dimensions of $30 \times 50 \times 50$ Å. Approximating the two domains by two spherical elements of equal mass, we compared our data to the calculated oligomeric structures is Ref. 19. The measured rotational correlation time $\tau_{exp} = 32.7$ ns of ferredoxin–NADP$^+$ reductase in the reduced state shows a very good agreement with the calculated value of $\tau_1 = 34.3$ ns for a 'dimer' model of two equal spheres. The significantly faster decay time of the oxidized protein compared to the model structure indicated that the axial ratio a/b of the oxidized protein was smaller than 2. The two spheres, both protein domains, seem to overlap which would result in the kidney-shaped structure obtained in x-ray studies.

The binary ferredoxin/ferredoxin–NADP$^+$ reductase complex was approximated as a trimer of 47 kDa with three spherical elements of equal mass, two representing the ferredoxin–NADP$^+$ reductase as above and the additional one representing ferredoxin. The expected rotational correlation times for the three elements were calculated in a 'rod' or a 'triangle' arrangement. The theoretical value of $\tau_1 = 74$ ns for an assumed rodlike structure is not consistent with our data for the complex of 34 ns (oxidized) and 37 ns (reduced). However, these correlation times fit fairly well to the triangle approximation with an expected time constant of 35 ns.

The above results indicate that both ferredoxin–NADP$^+$ reductase and its complex with ferredoxin have distinct conformations in the oxidized and reduced state. According to the interpretation of our hydrodynamic data the shape of the reduced enzyme can be approximated by an oligomer-like structure of two spheres. After transition to the oxidized state the centers of the two domains are more close together, rendering a structure of two overlapping spheres with an axial ratio $a/b < 2$ (in agreement with Ref. 12).

From our hydrodynamic data we can exclude the possibility that ferredoxin binds to ferredoxin–NADP$^+$ reductase with a stoichiometry higher than 1, since even at a 5-fold excess of ferredoxin only a 1 : 1 complex was observed. Both proteins most likely form a triangular structure, where ferredoxin is bound between the two domains of the flavoprotein (see Fig. 8). In the oxidized state ferredoxin seems to be more deeply immersed in ferredoxin–NADP$^+$ reductase, whereas upon reduction ferredoxin seems to protrude more. However, the complex was rather stable and did not dissociate even at higher ionic strength (≤ 100 mM). This suggests that the catalytic unit at the terminal end of the electron transport chain is the binary complex between ferredoxin and ferredo-

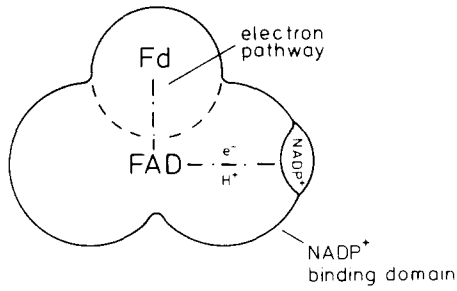

Fig. 8. Model structure of the oxidized binary complex of ferredoxin–$NADP^+$ reductase and ferredoxin as proposed from the analysis of the hydrodynamic data. Fd, ferredoxin.

xin–$NADP^+$ reductase rather than the flavoprotein alone. Therefore proposed reaction schemes, including association and dissociation of ferredoxin [10], seem to be unlikely. Moreover, our results support the concept that ferredoxin steadily bound to ferredoxin–$NADP^+$ reductase might provide a direct electron flow from the electron transport chain (PS I) to $NADP^+$ [11,16,40]. This concept is also supported by reports which indicate that thylakoid membranes contain two independent binding sites for ferredoxin, one at the membrane-bound reductase and the second at PS I [40]. Also it seems unlikely that 'free' ferredoxin simply acts as a shuttle for redox equivalents from or to PS I or to cytochrome *b/f* complex [22,26]. Finally it is tempting to speculate on some features of the model structure for the ferredoxin/ferredoxin–$NADP^+$ reductase complex shown in Fig. 8. The FAD moiety in the FAD domain of the flavoprotein seems to be located near the center of the enzyme (this still has to be proven by x-ray diffraction analysis) and the flavin is exposed to the solvent with a positively charged site [10,16]. In the iron-sulfur protein the iron-sulfur cluster is also exposed at the surface [27–29] with a net negative charge. In the structure shown in Fig. 8 the exposed centers of the two proteins come in close contact thereby facilitating direct electron transfer between the two proteins. The nucleotide binding fold in the $NADP^+$ binding domain is close to the FAD in order to allow direct electron transfer from 2Fe-2S via FAD to $NADP^+$.

Acknowledgements

Financial support of the Deutsche Forschungsgemeinschaft SFB 171/B2 is gratefully acknowledged. Preparation of the figures by H. Kenneweg and M. Meyer is very much appreciated. We thank Prof. Dr. W. Junge for generous support and comments on the manuscript. Special thanks from E.C.A. to Dr. S. Engelbrecht.

References

1 Zanetti, G. and Curti, B. (1980) Methods Enzymol. 69, 250–255.
2 Carrillo, N. and Vallejos, R.H. (1987) in Current Topics in Photosynthesis, (Barber, J., ed.), Vol. 8, Chapter 10, Elsevier, Amsterdam.
3 Carrillo, N. and Vallejos, R.H. (1982) Plant. Physiol. 69, 210–213.
4 Vallon, O., Wollman, F.A. and Olive, J. (1987) Prog. Photosynth. Res. 2, 329–332.
5 Vallejos, R.H., Ceccarelli, E. and Chan, R. (1984) J. Biol. Chem. 259, 8048–8051.
6 Ceccarelli, E.A., Chan, R.L., and Vallejos, R.H. (1985) FEBS Lett. 190, 165–168.
7 Foust, G.P., Mayhew, S.G. and Massey, V. (1969) J. Biol. Chem. 244, 964–970.
8 Shin, M. (1973) Biochim. Biophys. Acta 292, 13–19.
9 Bhattacharyya, A.K., Meyer, T.E. and Tollin, G. (1986) Biochemistry 25, 4655–4661.
10 Batie, C.J. and Kamin, H. (1984) J. Biol. Chem. 259, 8832–8839.
11 Wagner, R., Carillo, N., Junge, W. and Vallejos, R.H. (1982) Biochim. Biophys. Acta 680, 317–330.
12 Sheriff, S. and Heriott, J.R. (1981) J. Mol. Biol. 145, 441–451.
13 Karplus, P.A., Walsh, K.A. and Herriott, J.R. (1984) Biochemistry 23, 6576–6583.
14 Wagner, R., Carillo, N., Junge, W. and Vallejos, R.H. (1981) FEBS Lett. 131, 335–340.
15 Provencher, S.W. (1976) Biophys. J., 1627–1641.
16 Zanetti, G., Aliverti, A. and Curti, B. (1984) J. Biol. Chem. 259, 6153–6157.
17 Wagner, R. (1985) in Recent Advances in Biological Membrane Studies (Packer, L., ed.), Plenum Publishing Corp., New York.
18 Apley, E.C., Wagner, R. and Engelbrecht, S. (1985) Anal. Biochem. 150, 145–154.
19 Garcia Bernal, J.M. and Garcia de la Torre, J. (1981) Biopolymers 20, 129–139.
20 Wagner, R., Engelbrecht, S. and Andreo, C.S. (1985) Eur. J. Biochem. 147, 163–170.
21 Sedmak, J.J. and Grossberg, S.E. (1977) Anal. Biochem. 79, 544–552.
22 Haehnel, W. (1984) Annu. Rev. Plant Physiol. 35, 659–693.
23 Gozzer, C., Zanetti, G., Galliano, M., Sacchia, G.A.,

Minchiotti, L. and Curti, B. (1977) Biochim. Biophys. Acta 485, 278–290.
24 Cherry, R.J. (1979) Biochim. Biophys. Acta 559, 289–327.
25 Miner, C.S. and Dalton, N.N. (1953) Glycerol, Reinhold Publ. Corp., New York.
26 Clark, R.D., Hawkesford, M.J., Coughlan, S.J., Bennett, J. and Hind, G. (1984) FEBS Lett. 174, 137–142.
27 Yasunobu, K.T. and Tanaka, N. (1973) in Iron Sulfur Proteins (Lovenberg, W., ed.), Vol. II, pp. 29–130, Academic Press, New York.
28 Fukuyama, K., Hase, T., Matsumoto, S., Tsukihara, T., Katsube, Y., Tanaka, N., Kakudo, M., Wada, K. and Matsubara, H. (1980) Nature (Lond.) 286, 522–524.
29 Tsukihara, T., Fukuyama, K., Nakamura, M., Katsube, Y., Tanaka, N., Kakudo, M., Wada, K., hase, T. and Matsubara, H. (1981) J. Biochem. (Tokyo) 90, 1763–1773.
30 Tao, T., Nelson, J.H. and Cantor, C.R. (1970) Biochemistry 9, 3514–3523.
31 Batie, C.J. and Kamin, H. (1986) J. Biol. Chem. 261, 11214–11223.
32 Segel, I.H. (1975) Enzyme Kinetics, J. Wiley & Sons, New York.
33 Bookjans, G. and Böger, P. (1978) Arch. Biochem. Biophys. 190, 459–465.
34 Garnier, J., Osguthorpe, D.J. and Robson, B. (1978) J. Mol. Biol. 120, 97–120.
35 Sasagawa, T., Okuyama, T. and Teller, D.C. (1982) J. Chromatogr. 240, 329–340.
36 Schulz, G.E. and Schirmer, R.H. (1979) Principles of Protein Structure, Springer-Verlag, New York.
37 Kabsch, W. and Sander, C. (1983) FEBS Lett. 155, 179–182.
38 Hogan, D.L., Kraemer, K.L. and Isenberg, J.I. (1982) Anal. Biochem. 127, 17–24.
39 Zanetti, G. (1976) Biochim. Biophys. Acta 445, 14–24.
40 Merati, G. and Zanetti, G. (1987) FEBS Lett. 215, 37–40.
41 Chan, L.R., Carrillo, N. and Vallejos, R.H. (1985) Arch. Biochem. Biophys. 240, 172–177.